Size matters: An analytical study on the role of tissue size in spatiotemporal distribution of morphogens unveils a transition between different Reaction-Diffusion regimes.

Alberto S. Ceccarelli[1], Augusto Borges[1,2,3] & Osvaldo Chara[1,4]

[1] Systems Biology Group, Institute of Physics of Liquids and Biological Systems, National Scientific and Technical Research Council, University of La Plata, La Plata, Argentina

[2] Research Unit of Sensory Biology & Organogenesis, Helmholtz Zentrum München, Munich, Germany

[3] Graduate School of Quantitative Biosciences (QBM), Munich, Germany

[4] Center for Information Services and High Performance Computing, Technische Universität Dresden, Dresden, Germany

* Corresponding author:

E-mail: osvaldo.chara@tu-dresden.de, ochara@iflysib.unlp.edu.ar (OC)

Web: http://sysbioiflysib.wordpress.com/

Abstract:

The reaction-diffusion model constitutes one of the most influential mathematical models to study the distribution of morphogens spreading within tissues. Despite its widespread appearance, the role that the finitude of the tissue plays in the spatiotemporal morphogen distribution predicted by the model has not been unveiled so far. In this study, we investigated the spatiotemporal distribution of a morphogen predicted by a reaction-diffusion model in a 1D finite domain as a proxy to simulate a biological tissue. We analytically solved, for the first time to our knowledge, the model assuming morphogen produced *de novo* within a finite domain and compared it with the scenario considering an infinite domain, which was previously solved. We explored the only relevant parameter in the reduced model, the tissue length in units of a characteristic reaction-diffusion length, and fully characterized the model behavior in terms of: i) geometrical aspects of the spatial distributions and ii) kinetic features derived from the time elapsed to reach the steady state. We found a critical tissue size that we estimated as ~3.3 characteristic reaction-diffusion lengths, above which the model assuming the infinite domain could suffice as a reasonable approximation. In contrast, for tissues smaller than the critical size, the error of assuming an infinite domain could rapidly accumulate, indicating that the model assuming finite domains is a better description. This new solution could replace the one used to estimate diffusion coefficients and degradation constants during the analysis of Fluorescence Recovery After Photobleaching (FRAP) experiments and it could also help to improve the performance of multiscale computational approaches, which involve a morphogen dynamics scale, typically modeled with a reaction diffusion scheme. These findings could drive new modeling strategies to understand tissue morphogenesis as well as cancer invasion, among many other relevant problems in biology and medicine.

Introduction

In their transition towards maturity, tissues are crucially regulated by molecules known as morphogens, whose precise spatiotemporal distribution triggers the downstream changes in protein expression responsible for the exact differentiation patterns. Nevertheless, tissues are not only an inert scaffold upon which morphogens spread, but they are also fully responsible for the morphogen uptake or their transformation by means of specific biochemical reactions. The problem of how a morphogen propagates over a tissue while it is being eliminated was mathematically encoded in the exquisite reaction-diffusion model by the great Alan Turing, who coined the "morphogen" neologism to illustrate its character of "form generator" [1].

The reaction-diffusion model constitutes one of the most influential quantitative approaches within developmental biology. From the aforementioned Turing´s seminal article and the study from Gierer and Meinhardt [2], a progressive wealth of reaction-diffusion models were developed, paving the way to become an essential and pivotal concept to understand tissue morphogenesis [3,4,5,6]. The model was extensively used to investigate distributions of morphogens in a variety of tissues and organisms such as *Drosophila melanogaster* wing imaginal disc [7], chick limb [8] and the stripe pattern of *Danio rerio* [9] among other examples.

Previous studies have analytically investigated this model assuming an infinite domain [10,11]. Although the model relied on the idea that the reaction-diffusion characteristic length of the morphogen pattern was reasonably smaller than the domain, it is clear that biological tissues do not entail infinite lengths. Other reports investigated the model assuming a finite domain by using numerical approaches [7,12]. While some of these studies analytically explored the steady state [13,14], an analytical solution for the reaction-diffusion model of a morphogen formed *de novo* with finite domains that also include the transient regimes is, to our knowledge, still pending. Moreover,

the role played by the size of the domain in the spatiotemporal patterning predicted by this model has not yet been elucidated.

In this study, we present the analytical solution of a reaction-diffusion model describing *de novo* formation of a morphogen and its spread within a finite domain, representing a more realistic tissue. We analytically investigated the behavior of the model, in terms of a reduced parameter, representing the tissue length in units of a characteristic reaction-diffusion length. We fully characterized the model for finite domains in terms of morphological aspects of the spatial distributions and the time to reach the steady state to finally compare them with the corresponding predictions from the model assuming an infinite domain. We found a critical tissue size above which both model variants coincide. Importantly, below this critical size, the model for finite domains becomes a better approximation.

Results

2.1. The reaction-diffusion model in the infinite domain

Here we briefly summarize the well-known reaction-diffusion model assuming an infinite domain and its analytic solution [10,11]. Within this model, it is assumed that the dynamics of the morphogen are faster than the proliferation rate of the tissue cells and, as a consequence, advective effects can be neglected. Otherwise, an advective term could be included to the model [15]. Since during developmental process tissues usually organize along a particular axis [16,17], this model is studied in a one dimensional setting [10,11]. It is assumed that the morphogen concentration $C_1(x,t)$ can diffuse with a diffusion coefficient *D* and is linearly degraded with a rate *k*.

$$\frac{\partial C_1(x,t)}{\partial t} = \mathrm{D}\frac{\partial^2 C_1(x,t)}{\partial x^2} - kC_1(x,t) \qquad \text{(Eq. 1)}$$

It is considered that there is no morphogen at the beginning, that is, the initial condition is:

$$C_1(x\,, t = 0) = 0 \qquad \text{(Eq. 2)}$$

The only source of morphogen is a constant flux *q* located at the origin, represented by the first boundary condition:

$$\frac{dC_1}{dx}(x\ = 0, t) = -\frac{q}{D} \qquad \text{(Eq. 3)}$$

In this model, it can be assumed that there is a sink in the tip of the tissue absorbing the morphogen and assumes that the spatial domain is infinite:

$$\lim_{x\to\infty} C_1(x\,, t) = 0 \qquad \text{(Eq. 4)}$$

This model given by Eqs. 1-4 was extensively investigated by other authors, and the solution is [10,11]:

$$C_1(x,t) = \frac{q}{\sqrt{Dk}} e^{-\frac{x}{\sqrt{\frac{D}{k}}}} \left[1 - \frac{1}{2} erfc\left(\sqrt{kt} - \frac{x}{2\sqrt{Dt}}\right) - \frac{1}{2} e^{\frac{2x}{\sqrt{\frac{D}{k}}}} erfc\left(\sqrt{kt} + \frac{x}{2\sqrt{Dt}}\right) \right] \qquad \text{(Eq. 5)}$$

Where $erfc(x)$ is the complementary error function.

Space and time variables can be rewritten in terms of the following dimensionless variables $\varepsilon = \frac{x}{\sqrt{\frac{D}{k}}}$ and $\tau = kt$. Consequently, the morphogen flux at the tissue origin can be rewritten as $S = \frac{q}{\sqrt{Dk}}$ and the concentration as $C(\varepsilon, \tau) = \frac{C_1(\varepsilon,\tau)}{S}$. With this nondimensionalization, model equations (Eq. 1-4) take the form:

$$\frac{\partial C}{\partial \tau} = \frac{\partial^2 C}{\partial \varepsilon^2} - C \qquad \text{(Eq. 6)}$$

$$C(\varepsilon\,, \tau = 0) = 0 \qquad \text{(Eq. 7)}$$

Where the morphogen source at the tissue origin, in nondimensional units, $\varepsilon = 0$, is:

$$\frac{dC}{d\varepsilon}(\varepsilon\ = 0, \tau) = -1 \qquad \text{(Eq. 8)}$$

And a morphogen sink at infinite in the nondimensionalized units is now:

$$\lim_{\varepsilon \to \infty} C(\varepsilon\,, \tau) = 0 \qquad \text{(Eq. 9)}$$

Which leads to this solution:

$$C(\varepsilon, \tau) = e^{-\varepsilon} \left[1 - \frac{1}{2} erfc\left(\sqrt{\tau} - \frac{\varepsilon}{2\sqrt{\tau}}\right) - \frac{1}{2} e^{2\varepsilon} erfc\left(\sqrt{\tau} + \frac{\varepsilon}{2\sqrt{\tau}}\right) \right] \qquad \text{(Eq. 10)}$$

2.2. The reaction-diffusion model in finite domains: an analytical solution

The previous model variant entails an infinite domain (Eqs. 4 and 9). Since biological tissue sizes require a finite domain, we decided to replace the condition imposed by Eq. 4 with:

$$C_1(x = L, t) = 0 \qquad \text{(Eq. 11)}$$

Where L is the length of the tissue. To our knowledge, the general solution for any given L is yet unknown.

We defined the quantity $R = \frac{L}{\sqrt{\frac{D}{k}}}$, which is the only model parameter. This quantity represents the tissue length L in units of the characteristic reaction-diffusion length λ, defined as $\lambda = \sqrt{\frac{\mathrm{D}}{k}}$ [18,19]. Thus, the second boundary condition for this model in nondimensionalized units is:

$$C(\varepsilon = \mathrm{R}, \tau) = 0 \qquad \text{(Eq. 12)}$$

This equation replaces Eq. 9 in the section 2.1 assuming the finitude of the tissue.

We found the analytical solution of the general model for finite tissues (Eqs. 6-8 and 12) in the nondimensionalized units to be as follows (see S1 text for the demonstration):

$$C(\varepsilon, \tau) = \left(\frac{e^{-\varepsilon}}{1+e^{-2R}} - \frac{e^{\varepsilon}}{1+e^{2R}}\right) + \sum_{j=0}^{\infty} -\frac{2}{R}\frac{cos\left(\frac{\left(j+\frac{1}{2}\right)\pi\varepsilon}{R}\right)}{\left(\frac{\left(j+\frac{1}{2}\right)\pi}{R}\right)^2+1} e^{-\left[\left(\frac{\left(j+\frac{1}{2}\right)\pi}{R}\right)^2+1\right]\tau} \qquad \text{(Eq. 13)}$$

Moreover, we also found the solution for different boundary conditions such as assuming a non-null flux in $\varepsilon = 0$ and a zero flux in $\varepsilon = R$ as well as a fixed non-null concentration in $\varepsilon = 0$ and a null concentration in $\varepsilon = R$ (see S1 text). To further corroborate the analytical solution, we implemented the model numerically, by using a finite differences scheme (see S1 text). Our results indicate that the analytical solution is in agreement with numerical simulations (Fig. 1 in S1 Text).

128 **2.3 Transient morphogen distributions are qualitatively different between the model of infinite**
129 **domain and the model of finite domains when they are of the order of the characteristic length**
130 **λ or smaller.**

131 We decided to compare the reaction-diffusion model assuming a finite tissue *versus* an infinite
132 domain. With the selected nondimensionalization, the latter does not have any free parameters. In
133 contrast, the finite model has only one free parameter, *R*, which represents the tissue size in units
134 of the characteristic length of the morphogen profile λ. By using our analytical solution for the model
135 of finite tissues (Eq. 13), we explored the predicted morphogen spatial profiles at different tissue
136 sizes (*i.e.*, varying *R*) and compared them with those calculated from the previously known solution
137 assuming an infinite domain (Eq. 10), at three different time points (Fig. 1). We observed that the
138 morphogen concentrations predicted by the model assuming an infinite domain are higher than
139 those predicted by the model assuming a finite domain (Fig. 1 A, B). For large enough tissue lengths,
140 morphogen profiles predicted by both models are indistinguishable at each time point, as expected
141 (Fig. 1 C and Fig 1 D). Hence, the previously reported model assuming an infinite domain is a
142 reasonable description of the dynamics of morphogen profiles for larger tissues. However, when
143 addressing a tissue whose length is of the order of the characteristic length λ or smaller, the model
144 introduced in the present work is a more accurate description.

145 Moreover, we observed that large tissues lead to morphogen spatial distributions temporarily
146 separated. In contrast, spatial distributions at different time points are indistinguishable in shorter
147 tissues, suggesting that they already approached the steady state (Fig. 1A). This result would
148 indicate that the larger the tissue, the longer the time necessary to reach the morphogen spatial
149 distribution at the steady state (see also sections 2.4 and 2.6).

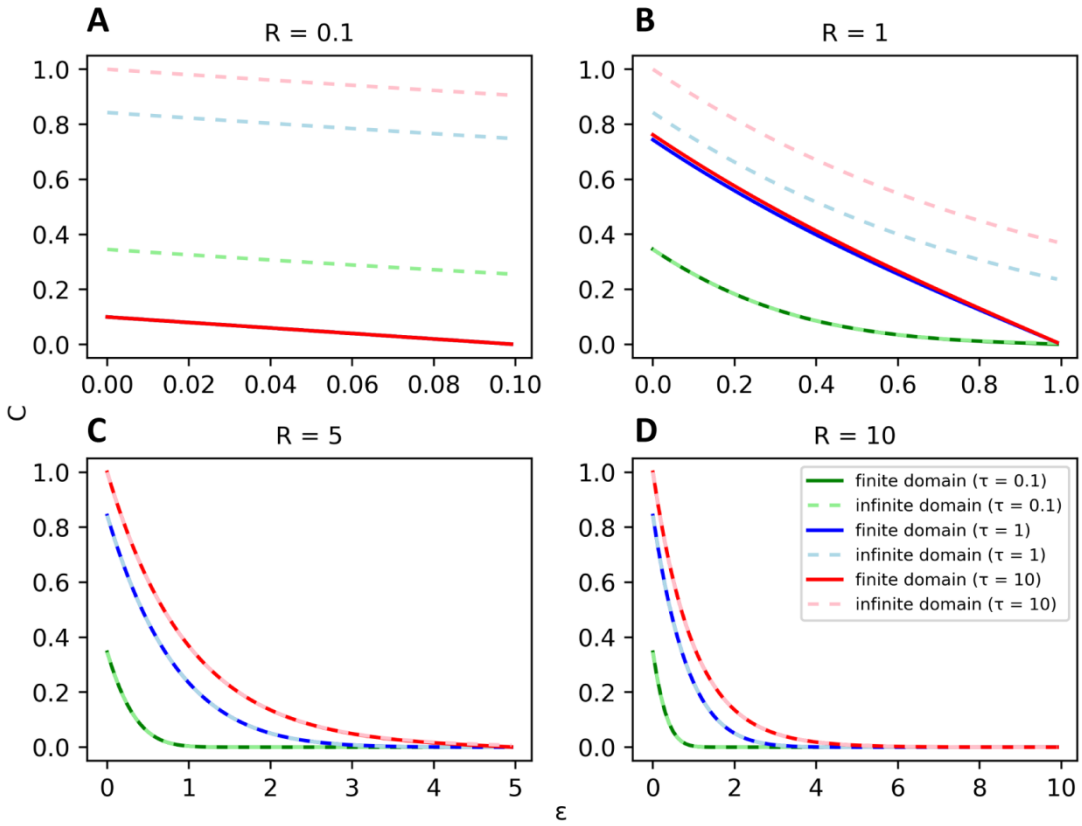

Figure 1. The morphogen spatial profile predicted from the reaction-diffusion model assuming finite domains at lengths larger than the critical size converges to the profile predicted from the model assuming an infinite domain. Morphogen spatial profiles of the reaction-diffusion model assuming finite domains considering that the normalized tissue sizes *R* are **A)** 0.1, **B)** 1, **C)** 5 and **D)** 10, respectively, are depicted at three different times τ = 0.1, 1 and 10 (solid lines). The profiles from the model assuming infinite domains are also shown at the same times (dashed lines). *C*, ε and τ represent the normalized morphogen concentration, space and time, respectively. In panel **A)**, all spatial concentration profiles for finite domain overlap.

2.4. Steady state morphogen spatial distributions

The morphogen spatial distribution assuming an infinite domain at the steady state ($C_{ss}^{infinite}(\varepsilon)$) is well known [10,11] and with our nondimensionalization it is the following exponential spatial decay:

$$C_{ss}^{infinite}(\varepsilon) = e^{-\varepsilon} \qquad \text{(Eq. 14)}$$

We calculated the steady state solution for our model of finite tissues, $C_{ss}^{finite}(\varepsilon)$, (S1 text):

$$C_{ss}^{finite}(\varepsilon) = \left(\frac{e^{-\varepsilon}}{1+e^{-2R}} - \frac{e^{\varepsilon}}{1+e^{2R}}\right) \qquad \text{(Eq. 15)}$$

Increasing the tissue size in this model modifies the steady state profile, augmenting the maximum concentration at the origin and leading to a transition from a linear to an exponential curve (Fig. 2), in agreement with the results observed at any time (Fig. 1). Precisely, the limits when the tissue size tends to zero and infinite are respectively:

$$\lim_{R\to 0} C_{SS}^{finite}(\varepsilon) = \frac{1}{2}(e^{-\varepsilon} - e^{\varepsilon}) \cong -\varepsilon \qquad \text{(Eq. 16)}$$

$$\lim_{R\to \infty} C_{SS}^{finite}(\varepsilon) = e^{-\varepsilon} = C_{ss}^{infinite}(\varepsilon) \qquad \text{(Eq. 17)}$$

Remarkably, the steady state morphogen distribution of the finite model converges to the exponential distribution predicted by the infinite domain when the tissue length tends to infinity.

Furthermore, by comparing the steady state solution (Eq. 15) with its complete solution (Eq. 13), we can re-write Eq. 13 as follows:

$$C(\varepsilon,\tau) = C_{ss}{}^{finite}(\varepsilon) + \sum_{j=0}^{\infty} -\frac{2}{R}\frac{cos\left(\frac{\left(j+\frac{1}{2}\right)\pi\varepsilon}{R}\right)}{\left(\frac{\left(j+\frac{1}{2}\right)\pi}{R}\right)^2+1} e^{-\left[\left(\frac{\left(j+\frac{1}{2}\right)\pi}{R}\right)^2+1\right]\tau} \qquad \text{(Eq. 18)}$$

Where the second term of Eq. 18 vanishes when the time τ tends to infinity. Therefore, the morphogen concentration can be expressed as the steady state solution plus a term that describes a transient contribution.

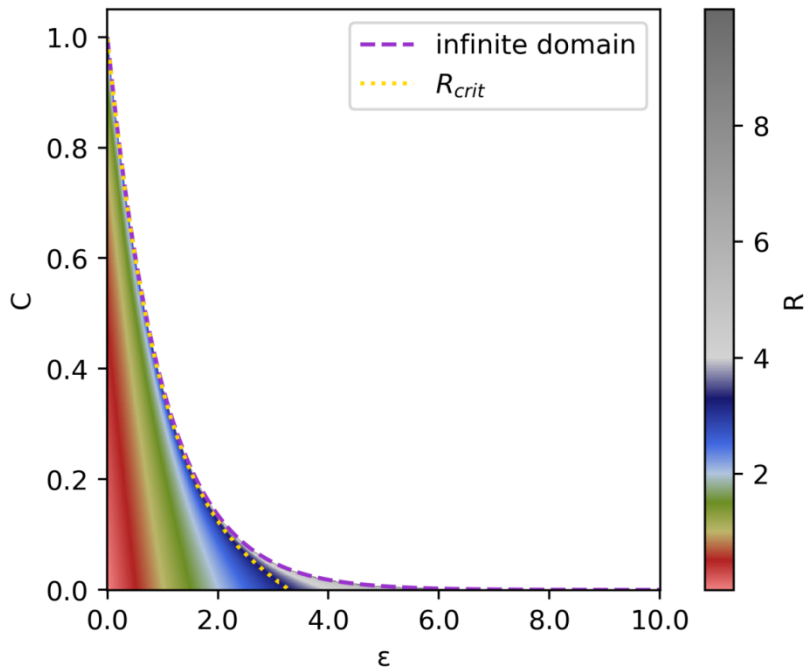

Figure 2. Morphogen spatial profile of the reaction-diffusion model assuming finite domains at the steady state transitions from a line-like to exponential-like spatial profile when the tissue size increases. Steady state profiles predicted from the reaction-diffusion model at different tissue sizes (R) are depicted. The steady state profile from the model assuming infinite domains and the critical tissue size R_{crit} (defined in section 2.5) are shown as dashed and dotted lines, respectively.

190 **2.5 Geometrical characterization of the morphogen spatial distributions**

191 The steady state profiles predicted by the model of finite tissues changed from linear to exponential
192 when increasing the tissue size as shown in section 2.4. In order to geometrically characterize the
193 shape of the spatial profiles in the steady state regime, we defined ε_{10} as the dimensionless spatial
194 position ε in which the morphogen concentration is 10 % of the concentration at the origin. When
195 using this definition in the model assuming infinite domains, we obtain (see S1 text for details):

196 $$\varepsilon_{10} = ln(10) \cong 2.3 \qquad \text{(Eq. 19)}$$

197 While for the model of finite tissues (see S1 text for details):

198 $$\varepsilon_{10} = R - \operatorname{arcsinh}\left(\frac{sinh(R)}{10}\right) \qquad \text{(Eq. 20)}$$

199 Thus, in the limit of small tissues, ε_{10} shows a linear dependence with the tissue size. However,
200 when the tissue tends to infinity, ε_{10} becomes independent of the precise tissue size, reaching a
201 plateau (Fig. 3). Additionally, when tissue size tends to infinity, in Eq. 20, ε_{10} recovers the value from
202 the infinite model calculated in Eq. 19.

203 We wonder whether it is possible to establish a cut-off size to distinguish both regimes. To answer
204 this question, we explore under what conditions, the shape of the morphogen spatial distribution
205 depends on the tissue size. More precisely, we asked under what critical tissue size R_{crit} the
206 geometrical observable ε_{10} would transition from linearly depending on the tissue size to becoming
207 independent of it. To this end, we Taylor-expanded ε_{10} and arbitrarily looked for the $R = R_{crit}$ upon
208 which the second non-zero term of the series would be about 20 % of the first linear term (See S1
209 text for details). Our results show that the critical tissue size separating both regimes is about 3
210 times the characteristic length λ $(R_{crit} \approx 3.3)$.

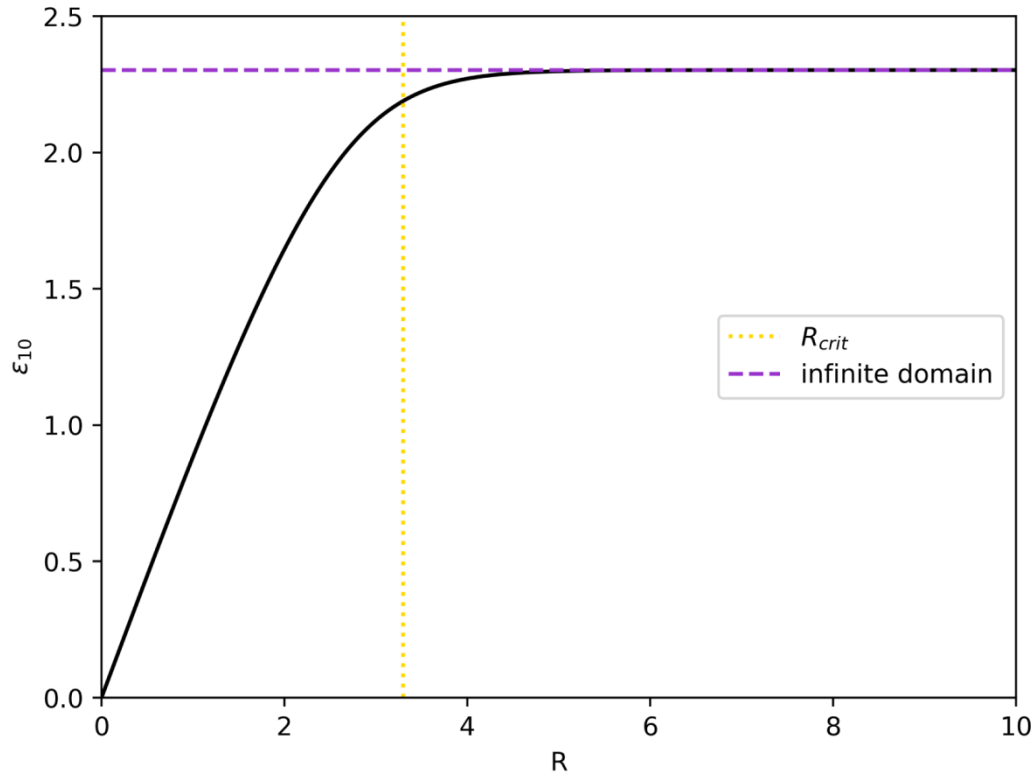

Figure 3. The geometrical factor ε_{10} characterizing the steady state spatial profiles of the reaction-diffusion model assuming finite domains (solid line) linearly grows with the tissue size (*R*, tissue length in nondimensional units) until it converges to the ε_{10} predicted from the model assuming an infinite domain (horizontal dashed line). ε_{10} is defined as the spatial position (ε) where the morphogen concentration is 10 % of its value at the origin. The vertical dotted line shows the critical tissue size R_{crit}.

The analysis of the dependency of ε_{10} with the tissue size can also be made before the morphogen distribution achieves the steady state. Although we could not find an analytical expression for this observable in the general case, we explored this dependency numerically (Fig. 4). We observed that, for each tissue size, ε_{10} increases in time until it reaches a plateau, which indicates that the spatial profile stabilizes in the steady state. Moreover, the time needed to reach the plateau monotonically

increases with the tissue size until $R \sim R_{crit}$. For larger tissue sizes, the time to reach the plateau converges to the prediction of the model for infinite domains (Fig. 4). This result is consistent with the fact that morphogen spatial distributions at different times are overlapped in smaller tissues and separated in larger ones (Fig. 1). This is a consequence of the second term of Eq. 18: the larger the tissue, the longer waiting times are required to vanish the exponential in the second term.

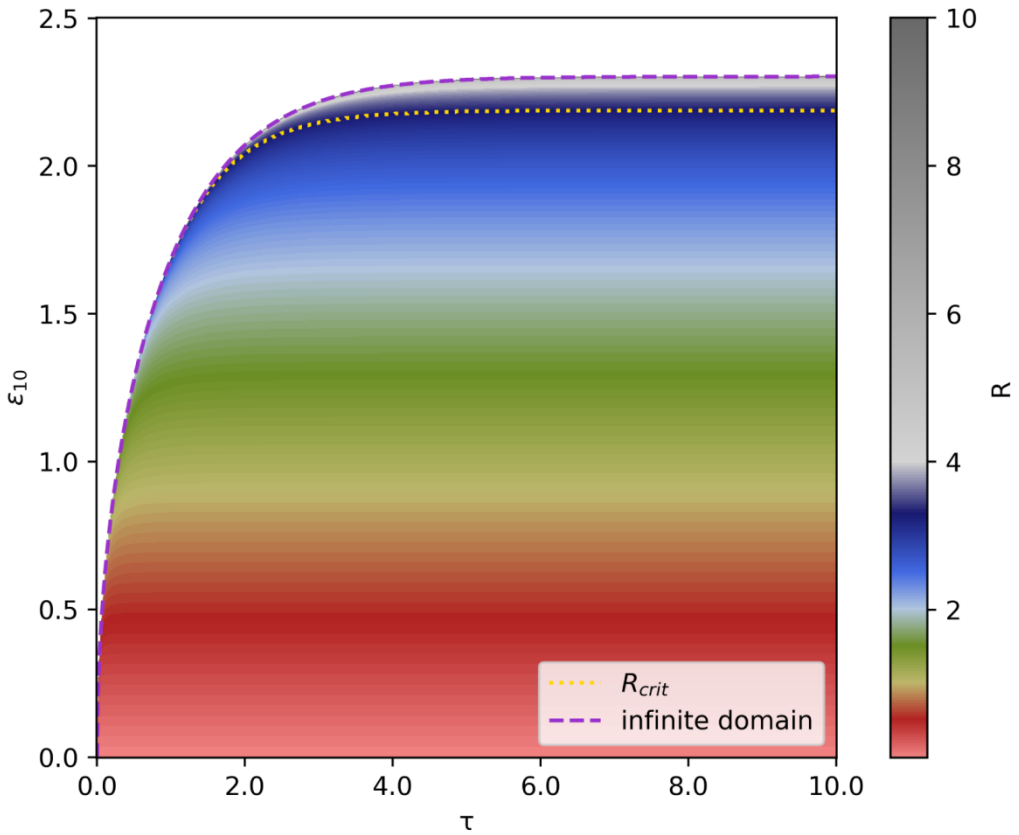

Figure 4. The larger the tissue, the longer the time to reach the steady state. Kinetics of the geometrical factor ε_{10} predicted from the model for finite tissues of different sizes (R, tissue length in normalized units). The kinetic of the factor ε_{10} of the model for an infinite domain is also shown (dashed line). ε_{10} is defined as the spatial position (ε) where the morphogen concentration is 10 % of its value at the origin. The dotted line shows the critical value R_{crit}.

2.6 Time to reach the steady state morphogen distribution

In Section 2.5 we suggested that the larger the tissue, the longer it takes the model to reach the steady state. To test this hypothesis, we took advantage of a method developed by Berezhkovskii and colleagues [11] to quantify the mean time (μ_τ) it takes a morphogen profile to reach its steady state. They applied this method to the reaction-diffusion model assuming an infinite domain and obtained (in our nondimensional units):

$$\mu_\tau(\varepsilon) = \frac{\varepsilon+1}{2} \qquad \text{(Eq. 22)}$$

That is, the mean time to reach the steady state is linear with the position within the infinite domain. We applied the same method to our reaction-diffusion model of finite tissues and obtained (see S1 text for details):

$$\mu_\tau(\varepsilon) = \sum_{j=0}^{\infty} -\frac{2}{R}\frac{cos\left(\frac{\left(j+\frac{1}{2}\right)\pi\varepsilon}{R}\right)}{\left[\left(\frac{\left(j+\frac{1}{2}\right)\pi}{R}\right)^2+1\right]^2}\frac{1}{\left(\frac{e^{-\varepsilon}}{1+e^{-2R}}-\frac{e^{\varepsilon}}{1+e^{2R}}\right)} \qquad \text{(Eq. 23)}$$

Thus, for our model, the mean time to reach the steady state not only depends on the position within the tissue but also on the tissue size.

To formally compare the mean times calculated from both reaction-diffusion models we also need to estimate a measure of the error. Hence, we calculated the standard deviation of the time to reach the steady state, σ_τ (see S1 text for details). For the model assuming an infinite domain, it reads:

$$\sigma_\tau(\varepsilon) = \frac{\sqrt{\varepsilon+2}}{2} \qquad \text{(Eq. 24)}$$

Which coincide with the already reported result by Ellery and colleagues [13]. In contrast, for the reaction-diffusion model for finite tissues, we obtain:

$$\sigma_\tau(\varepsilon) = \sqrt{\sum_{j=0}^{\infty} \frac{2}{R} \frac{cos\left(\frac{\left(j+\frac{1}{2}\right)\pi\varepsilon}{R}\right)}{\left[\left(\frac{\left(j+\frac{1}{2}\right)\pi}{R}\right)^2+1\right]^3} \frac{1}{\left(\frac{e^{-\varepsilon}}{1+e^{-2R}}-\frac{e^{\varepsilon}}{1+e^{2R}}\right)} - \left(\sum_{j=0}^{\infty} -\frac{2}{R} \frac{cos\left(\frac{\left(j+\frac{1}{2}\right)\pi\varepsilon}{R}\right)}{\left[\left(\frac{\left(j+\frac{1}{2}\right)\pi}{R}\right)^2+1\right]^2} \frac{1}{\left(\frac{e^{-\varepsilon}}{1+e^{-2R}}-\frac{e^{\varepsilon}}{1+e^{2R}}\right)}\right)^2} \quad \text{(Eq. 25)}$$

As with the mean, the standard deviation of the time necessary to reach the steady state not only depends on the positions along the tissue but also on the tissue size. At the origin of the tissue (ε = 0), both, μ_τ and σ_τ, increase with *R* until they converge toward $\frac{1}{2}$ and $\frac{\sqrt{2}}{2}$, respectively, when *R* tends to infinite (Fig. 5 A). These are precisely the expected values from the model assuming infinite domains evaluated at the tissue origin (Eqs. 22 and 24). Interestingly, the transition between the domains in which μ_τ and σ_τ depend on the tissue size and where they are independent of it coincides with the critical tissue size of about 3 λ determined in the previous section (compare Fig. 5 A with Fig. 3). The ratio between them, constituting the Coefficient of Variation $C_v(\varepsilon) = \frac{\sigma_\tau(\varepsilon)}{\mu_\tau(\varepsilon)}$, also experiences a transition near the critical tissue size until converging to $\sqrt{2}$ (Fig. 5 A).

For tissues smaller than the critical size, the mean time to achieve the steady state and its error in each position strongly depend on tissue size (Fig. 5 B). On the contrary, for tissue sizes higher than the critical tissue size, both magnitudes become independent of the size (Fig. 5 C). Importantly, for tissues smaller than the critical size, the steady state will be reached significantly faster than the prediction from the model assuming an infinite domain. For tissues larger than the critical size, both models agree in the time to achieve steady state (Fig. 5 B and C).

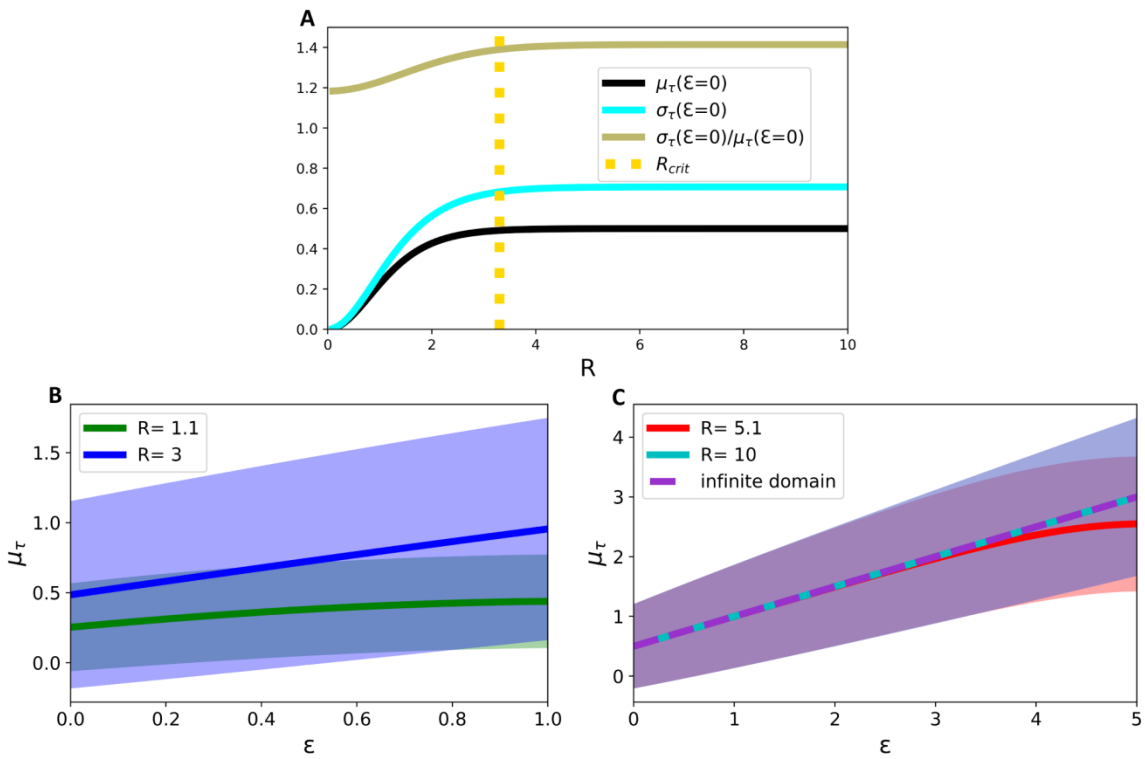

Figure 5. Critical tissue size separates two regimes of the time to reach the steady state. A) The mean time to reach the steady state (black line), the standard deviation (light blue line) and the variation coefficient (brown line) as a function of *R* predicted from the model assuming finite domains at $\varepsilon = 0$. The vertical dotted line indicates the critical tissue size R_{crit}. **B)** Spatial profile of the mean time to reach the steady state for *R* = 1.1 (green line) and *R* = 3 (blue line). The standard deviation (σ_τ) is represented by the shady areas surrounding the curves. **C)** Spatial profile of the mean time to reach the steady state for *R* = 5.1 (red line) and *R* = 10 (light blue line). The result for the model of an infinite domain is shown in violet dashed line. The standard deviation (σ_τ) is represented by the shady areas surrounding the curves.

279 **2.7 Finite *versus* infinite domains in the reaction-diffusion model used in the FRAP-based**
280 **determination of diffusion parameters**

281 Diffusion parameters of morphogens can be experimentally determined in tissues by using
282 Fluorescence recovery after photobleaching (FRAP) experiments [20, 21]. From this technique, D
283 and k are obtained indirectly by fitting the analytical solution of the model assuming an infinite
284 domain to experimental concentration measurements [17, 22]. Thus, we wondered if the election
285 of the model used in FRAP has an impact on the calculated D and k.

286 We tested, as a proof of principle, how good the estimation of the kinetic parameters (D and k) using
287 the infinite domain model is. We generated data points of concentration at the steady state as a
288 function of position. To this end, we rewrote the concentration at the steady state for the finite
289 tissue model (Eq. 15) in the original coordinate $x = \lambda\varepsilon$ and arbitrarily set $\lambda = 1$. Finally, we used this
290 equation to calculate the concentration as a function of the position for different values of L,
291 obtaining one data set for each L.

292 Then, we rewrote the concentration at the steady state for the infinite domain model (Eq. 14) in the
293 original coordinate x and performed a curve fitting for each of the data sets obtained using Eq. 15.
294 We used Eq. 14 in the original coordinate as fitting function and λ as the free parameter. We
295 obtained the predicted value of λ as a function of $R = L$ (Fig. 6). For large values of R the predicted λ
296 is approximately 1, which is in agreement with the value used to generate the data. In contrast, for
297 values of R smaller than R_{crit}, the predicted value of λ deviate from 1, converging to 0 for small values
298 of R. We concluded that both models can be used to infer the kinetic parameters D and k from FRAP
299 experiments, provided that tissue sizes are higher than R_{crit}. On the contrary, for tissues smaller than
300 this critical value, the model assuming finite domains is the best alternative.

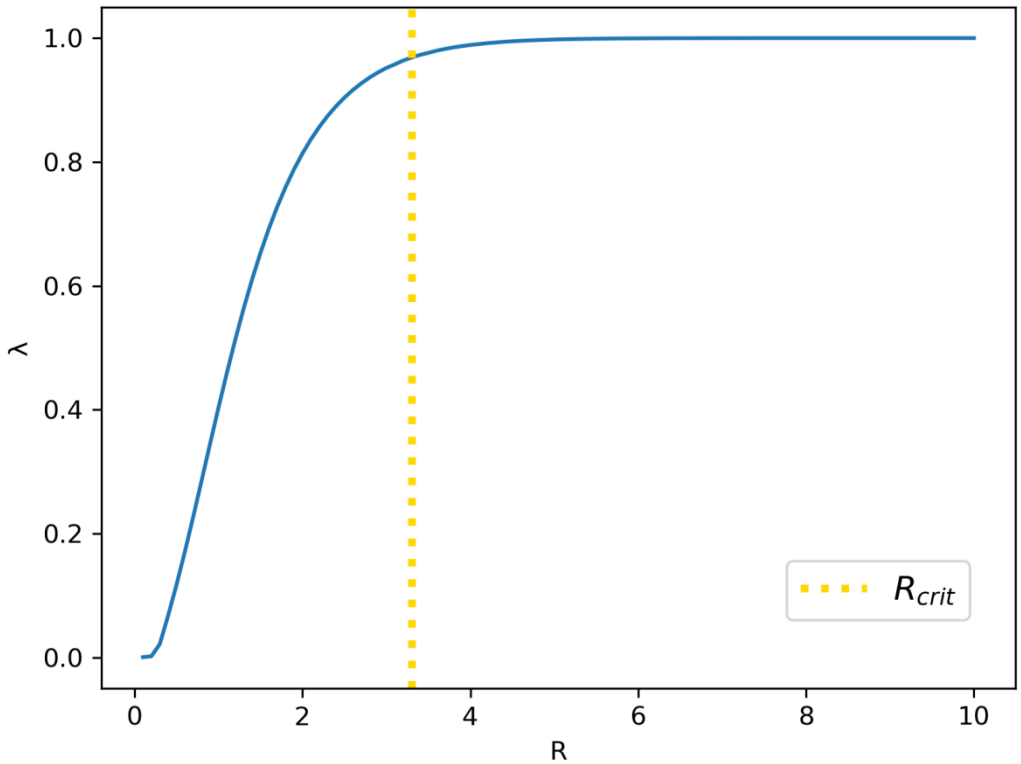

Figure 6. The reaction-diffusion model assuming an infinite domain does not correctly predict the characteristic length for tissues smaller than the critical size. The concentration of a morphogen in steady state was simulated with the model assuming finite domains along 101 equidistant positions from 0 to *L*, for different values of *L* going from 0.1 to 10. λ was arbitrarily set equal to 1. The simulated curves were fitted with the model assuming an infinite domain where λ was the only free fitting parameter. For large values of *R* the infinite domain model predicts correctly the value $\lambda = 1$. For R smaller than R_{crit} (depicted by the vertical yellow dotted line) the predicted λ goes to 0.

Discussion

Reaction-diffusion models were conceived in the seminal article of Alan Turing to hypothesize under what conditions heterogeneous patterns could emerge from a homogeneous one in tissue morphogenesis [1]. After the concept of positional information was posed by Lewis Wolpert [23], as illustrated by his well-known French Flag Problem ([24]; see also the review by Sharpe [25]), reaction-diffusion models resurfaced to account for mechanisms capable of generating spatial gradients that could serve as positional signals. Francis Crick was entertaining the hypothesis of reaction-diffusion signals as probable morphogenetic driving forces [26]. Reaction-diffusion models were specifically studied by Alfred Gierer and Hans Meinhardt to understand pattern formation in tissue development and regeneration [2]. Thereafter, a plethora of reaction-diffusion models were developed and proposed over the years to describe different morphogen gradients [27,28,29,30]. Some notable examples are Bcd in the syncytial *Drosophila* embryo [31], Dpp in developing wing imaginal disc in *Drosophila* [17], Fgf8 in the gastrulating *Danio rerio* embryo [32], among other examples. Despite the controversy of whether reaction-diffusion models represent an effective or accurate description of tissue pattern formation, these modeling framework became an essential construct to guide mathematical approaches in development [5,33] and regeneration [34].

In this study, we investigated the spatiotemporal distribution of a morphogen with a minimal reaction-diffusion model in a finite domain, as a proxy of a tissue. The solution of the model assuming an infinite domain has been already reported [10,11]. Although a number of reaction-diffusion models were previously considered to investigate morphogen gradients in finite domains, they were numerically simulated (see, for instance, [7,12], among other examples). The solution, assuming finite domains, to study the spatiotemporal distribution of a morphogen produced *de novo* in a tissue, to the authors' knowledge, was still pending. A similar model was considered to

investigate cell migration and proliferation of a population of precursor cells on a uniformly growing tissue by Simpson [35], based on the model of cell colonization in uniformly growing domains [36]. In his model, Simpson [35] explored a more general case of a growing domain, which can recapitulate the case of a fixed domain by setting the growth speed to zero. Nevertheless, because the model focused on cells instead of morphogens, it assumed a positive reaction term to account for cell proliferation and a non-zero initial condition, in contrast to our negative reaction term and our zero initial condition. Hence, imposing a zero initial condition in this previously reported model yields the null solution.

The analytical solution here reported could be instrumental in computational packages devoted to multi-scale modeling, which involve a signaling scale coupled with a cellular scale. Although their cellular layer could entail a Cellular Potts Model (CPM) [37, 38] in CompuCell3D [39] and MORPHEUS [40], or a vertex model [41, 42] in CHASTE [43], their signaling scale is typically modeled by a reaction-diffusion scheme. Since in these packages a finite domain is the only possible choice, they cannot avoid a numerical implementation. While our numerical results, based on a finite-difference algorithm cannot be distinguished from the analytical solution (Fig. 1 in S1 text), the last one is naturally more accurate and computationally more efficient (see S1 text), which could prove useful for multi-scale modeling implementations. Likewise, this new solution could help improve the calculation of recovery curves in FRAP experiments, as for tissues below the critical size R_{crit}, the model assuming finite domains is a better approximation.

Our results showed that the morphogen spatial distributions predicted by our model assuming finite domains depend on the only relevant model parameter: the normalized tissue size R. By determining the spatial position along the tissue where the morphogen concentration is 10 % of the source concentration (ε_{10}), we geometrically characterized the steady state spatial distribution. This characterization led us to find two regimes within the parameters space, separated by a critical

tissue size R_{crit} (Fig. 3 and Fig. 7C and 7D). For tissues longer than R_{crit}, the distributions are exponential-like and cannot be distinguished from those predicted from the model assuming an infinite domain (Fig. 2 and Fig. 7B). In this regime of the parameter space, the mean and standard deviation of the time to reach the steady state (evaluated at the tissue origin) do not change much with the tissue size and converged towards the corresponding values from the model assuming an infinite domain (Fig. 5 and Fig. 7F). When comparing the morphogen concentrations predicted by both models we found that the difference between them is mostly negligible (Fig. 8 A and B). Hence, the model assuming an infinite domain can be considered a good approximation of the model assuming finite domains for tissue sizes larger than R_{crit}.

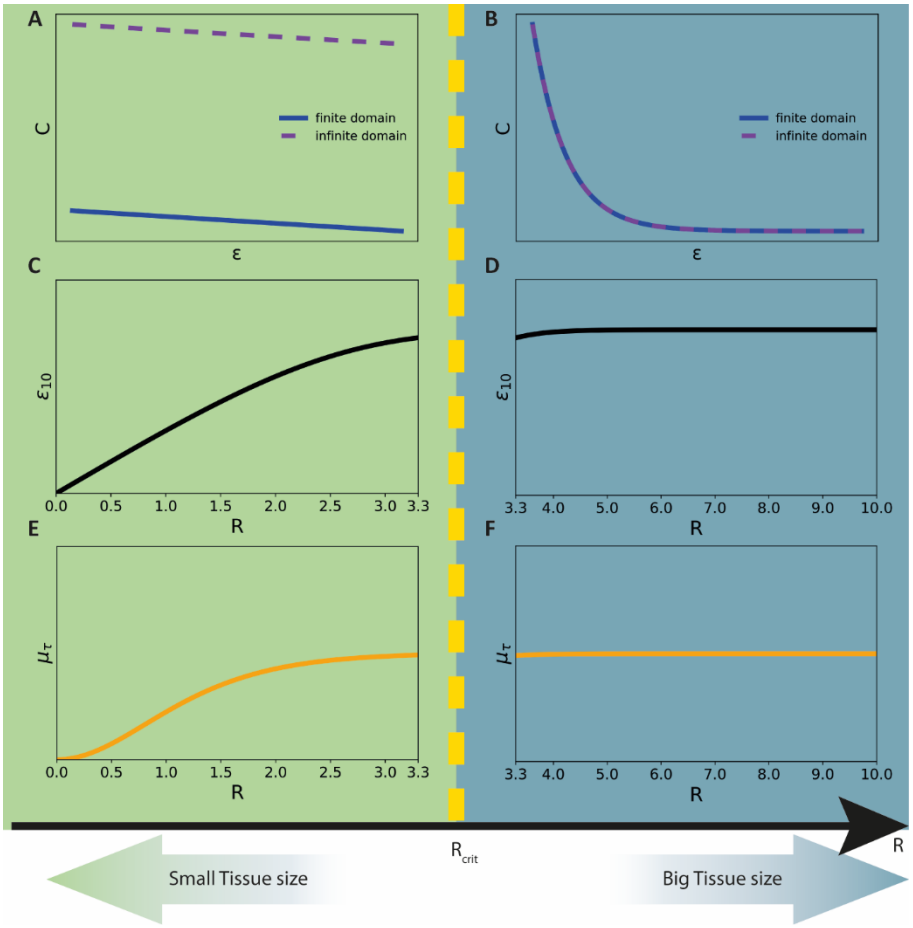

Figure 7. Transition between small and large tissues: Two reaction-diffusion regimes separated by a critical tissue size. Sketch summarizing the main differences between small and large tissue sizes. Spatial profiles of morphogen concentration *C* **(A, B)** and dependency of the geometrical factor ε_{10} **(C, D)** and the mean time to reach the steady state μ_τ **(E, F)** with the nondimensionalized tissue size *R*, for small (A, C, E) and large tissues (B, D, F). Critical tissue (R_{crit}) size depicted by the yellow dotted Vertical line.

In contrast, for tissues smaller than R_{crit}, the distributions tend to be linear and are clearly separated from those predicted with the model assuming an infinite domain (Fig. 2 and Fig. 7A). Furthermore, the time to reach the steady state strongly depends on the tissue size in this regime (Fig. 5 and Fig. 7E). In particular, the error of using the model assuming an infinite domain increases when ε tends to *R* and the smaller the tissue the higher the error accumulated over the entire tissue (Fig. 8 A and B) (See S1 text for details). Thus, our results indicate that to investigate tissues smaller than approximately 3 times the characteristic length λ, the model assuming finite domains should be used.

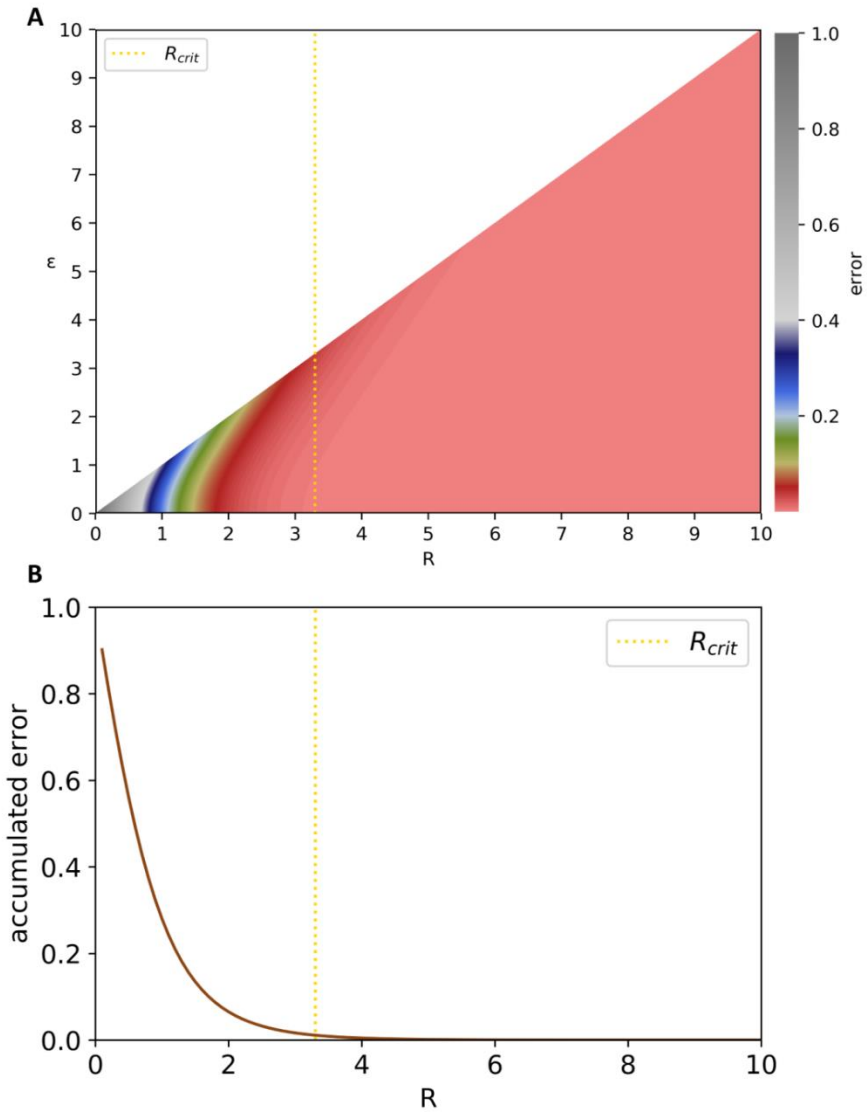

Figure 8. The reaction-diffusion model assuming a finite domain is a better approximation than the model assuming an infinite domain when the tissue size is smaller than the critical tissue size. A) Heat map showing the difference of morphogen concentration predicted from the reaction-diffusion model assuming a finite and the infinite domain as a function of the position within the tissue (ε) and the tissue size (R). This difference could be considered as the error committed when utilizing the standard model assuming the infinite domain at a given position ε from a tissue of size R. **B)** The difference calculated in (A) integrated over the tissue and normalized with R, as a function of R, representing the global error of using the standard model assuming the infinite domain when the tissue size is R. The vertical dotted line indicates the critical tissue size R_{crit}.

390 The critical tissue size provides a straightforward criterion to decide when to use any of the two
391 models presented here. As an example, the characteristic length of Wg was estimated in 6 μm in
392 the *Drosophila* wing disc, where the tissue size was about 50 μm [17]. The resulting $R \sim 8 > R_{crit}$
393 indicates that the model assuming an infinite domain is a reasonable approximation in this scenario.
394 A similar conclusion can be drawn when studying Dpp in the *Drosophila* haltere. For this morphogen,
395 the characteristic length and the tissue size can be estimated in ~ 10 and ~ 100 μm, respectively [7],
396 which leads to $R \sim 10 > R_{crit}$. In contrast, the last morphogen, Dpp, but in the *Drosophila* wing disc
397 has a characteristic length of 20 μm [17] which implies $R \sim 2.5 < R_{crit}$. As a consequence, the model
398 assuming finite tissues is the most correct approximation to describe morphogen propagation in
399 this scenario. Something similar occurs with Fgf8 in the *Danio rerio* embryo, whose characteristic
400 length was estimated as 200 μm while the tissue size is about 200 μm [32], from which a $R \sim 1 < R_{crit}$
401 can be calculated. By only looking at the previous examples, it is clear that there is no correlation
402 between the model selection and the morphogen under study, since the same morphogen, Dpp
403 dynamics is better explained with the model assuming finite domains in the *Drosophila* wing disc
404 while in the *Drosophila* haltere the model assuming an infinite domain is actually sufficient. The
405 same lack of correlation can be observed between the model selection and the tissue of interest.
406 Indeed, in the same tissue, *Drosophila* imaginal disc, Wg could be described with the model
407 assuming an infinite domain while Dpp requires the most precise model of finite domains.

408 In conclusion, we analytically solved the reaction-diffusion model assuming a more realistic finite
409 domain and compared it with the model of the infinite domain previously reported. Importantly, we
410 found two reaction-diffusion regimes for large and small tissues separated by a critical tissue size.
411 Above the critical size, the model assuming the infinite domain could suffice as a reasonable
412 approximation. In contrast, the error of assuming an infinite domain could rapidly accumulate in
413 smaller tissues, indicating that the model assuming finite domains is more accurate. Further studies

414 will be needed to unveil the spatiotemporal distribution of morphogens in tissues whose size is not
415 fixed. We speculate that the critical tissue size separating the two reaction-diffusion regimes could
416 be important to select the proper reaction-diffusion models in future strategies aimed to
417 understand tissue morphogenesis as well as cancer invasion, among many other relevant problems
418 in biology and medicine.

419

Computational methods.

In this article, the reaction-diffusion model assuming a finite domain and its comparison with the model assuming an infinite domain were studied. The analytical derivation of the reaction-diffusion model assuming a finite domain for different boundary conditions is presented in the section 1 in S1 text. Comparison between analytical and numerical solutions is described in the section 2 in S1 text. Steady state calculations, the geometrical characterization of the spatial distribution profiles given by ε_{10} and the estimation of the critical tissue size R_{crit} are shown in the sections 3, 4 and 5 in S1 text, respectively. Mean time to reach the steady state together with its standard deviation are in the section 6 in S1 text. Details on the error of assuming an infinite domain instead of a finite domain in the steady state solutions are in the section 7 in S1 text. Finally, the efficiency of the analytical solution *versus* the numerical one is analyzed in the section 8 in S1 text.

All model calculations were encoded in Python 3.7.3 and performed using numpy [44] and scipy [45] while visualization was executed with matplotlib [46] and seaborn [47]. The source codes for all the calculations and figures were implemented in supplementary notebooks using Jupyter Notebook (http://jupyter.org/) and can be found at: http://doi.org/10.5281/zenodo.4421327 [48].

Acknowledgements

We thank Diane Peurichard and Valeria Caliaro from the INRIA Paris - team MAMBA and the Laboratoire Jacques Louis Lions (LJLL)- Sorbonne Université, Juan José Gervasio from University of La Plata and the SysBio members of the Chara lab for their invaluable comments on this study.

440 **References**

441 1. Turing AM. The chemical basis of morphogenesis. Phil Trans R Soc Lond B. 1952 Aug
442 14;237(641):37-72. doi: 10.1098/rstb.1952.0012.

443 2. Gierer A, Meinhardt H. A theory of biological pattern formation. Kybernetik. 1972;12:30–39. doi:
444 10.1007/BF00289234.

445 3. Landge AN, Jordan BM, Diego X, Müllera P. Pattern formation mechanisms of self-organizing
446 reaction-diffusion systems. Dev Biol. 2020 Apr 1;460(1):2-11. doi: 10.1016/j.ydbio.2019.10.031.

447 4. Pally D, Pramanik D, Bhat R. An Interplay Between Reaction-Diffusion and Cell-Matrix Adhesion
448 Regulates Multiscale Invasion in Early Breast Carcinomatosis. Front Physiol. 2019 Aug 13;10:790.
449 doi: 10.3389/fphys.2019.00790.

450 5. Morelli LG, Uriu K, Ares S, Oates AC. Computational Approaches to Developmental Patterning.
451 Science. 2012 Apr 13;336(6078):187-191. doi: 10.1126/science.1215478.

452 6. Kondo S, Miura T. Reaction-Diffusion Model as a Framework for Understanding Biological Pattern
453 Formation. Science. 2010 Sept 24:329(5999);1616-1620. doi: 10.1126/science.1179047.

454 7. Wartlick O, Mumcu P, Kicheva A, Bittig T, Seum C, Jülicher F, et al. Dynamics of Dpp Signaling and
455 Proliferation Control. Science. 2011 Mar 4;331(6021):1154-1159. doi: 10.1126/science.1200037.

456 8. Dillon R, Othmer HG. A mathematical model for outgrowth and spatial patterning of the
457 vertebrate limb bud. J Theor Biol. 1999 Apr;197(3):295-330. doi: 10.1006/jtbi.1998.0876.

458 9. Asai R, Taguchi E, Kume Y, Saito M, Kondo S. Zebrafish leopard gene as a component of the
459 putative reaction-diffusion system. Mech Dev. 1999 Dec;89(1-2):87-92. doi: 10.1016/s0925-
460 4773(99)00211-7.

461 10. Bergmann S, Sandler O, Sberro H, Shnider S, Schejter E, Shilo BZ, et al. Pre-steady-state decoding
462 of the Bicoid morphogen gradient. PLoS Biol. 2007 Feb;5(2):e46. doi: 10.1371/journal.pbio.0050046.

463 11. Berezhkovskii AM, Sample C, Shvartsman SY. How long does it take to establish a morphogen
464 gradient? Biophys J. 2010 Oct 20;99(8):L59-61. doi: 10.1016/j.bpj.2010.07.045. Erratum in: Biophys
465 J. 2010 Nov 17;99(10):3505.

466 12. Michon F, Forest L, Collomb E, Demongeot J, Dhouailly D. BMP2 and BMP7 play antagonistic
467 roles in feather induction. Development. 2008 Aug;135(16):2797-805. doi: 10.1242/dev.018341.

468 13. Ellery AJ, Simpson MJ, McCue SW, Baker RE. Simplified approach for calculating moments of
469 action for linear reaction-diffusion equations. Phys Rev E Stat Nonlin Soft Matter Phys. 2013
470 Nov;88(5):054102. doi: 10.1103/PhysRevE.88.054102.

471 14. Rasolonjanahary M, Vasiev B. Scaling of morphogenetic patterns in reaction-diffusion systems.
472 J Theor Biol. 2016 Sep 7;404:109-119. doi: 10.1016/j.jtbi.2016.05.035.

473 15. Crampin EJ, Gaffney EA, and Maini PK. Reaction and diffusion on growing domains: Scenarios
474 for robust pattern formation. Bull Math Biol. 1999; 61:1093–1120. doi: 10.1006/bulm.1999.0131.

475 16. Gregor T, Bialek W, de Ruyter van Steveninck RR, Tank DW, Wieschaus EF. Diffusion and scaling
476 during early embryonic pattern formation. Proc Natl Acad Sci USA. 2005 Dec 20;102(51):18403-7.
477 doi: 10.1073/pnas.0509483102.

478 17. Kicheva A, Pantazis P, Bollenbach T, Kalaidzidis Y, Bittig T, Jülicher F, et al. Kinetics of morphogen
479 gradient formation. Science. 2007 Jan 26;315(5811):521-5. doi: 10.1126/science.1135774.

480 18. Oates AC, Gorfinkiel N, González-Gaitán M, Heisenberg CP. Quantitative approaches in
481 developmental biology. Nat Rev Genet. 2009 Aug;10(8):517-30. doi: 10.1038/nrg2548.

19. Wartlick O, Kicheva A, González-Gaitán M. Morphogen gradient formation. Cold Spring Harb Perspect Biol. 2009 Sep;1(3):a001255. doi: 10.1101/cshperspect.a001255.

20. Kicheva A, Bollenbach T, Wartlick O, Jülicher F, Gonzalez-Gaitan M. Investigating the principles of morphogen gradient formation: from tissues to cells. Curr Opin Genet Dev. 2012. doi: 10.1016/j.gde.2012.08.004.

21. Müller P, Rogers KW, Jordan BM, Lee JS, Robson D, Ramanathan S, et al. Differential Diffusivity of Nodal and Lefty Underlies a Reaction-Diffusion Patterning System. Science 2012. doi: 10.1126/science.1221920.

22. Axelrod D, Koppel DE, Schlessinger J, Elson E, Webb WW. Mobility measurement by analysis of fluorescence photobleaching recovery kinetics. Biophys J. 1976;16(9):1055-1069. doi:10.1016/S0006-3495(76)85755-4.

23. Wolpert L. Positional information and the spatial pattern of cellular differentiation. J Theor Biol. 1969 Oct;25(1):1-47. doi: 10.1016/s0022-5193(69)80016-0.

24. Wolpert L. Towards a Theoretical Biology. Vol.1 ed. C. H. Waddington, pp. 125 -133. Edinburgh: Edinburgh University Press; 1968.

25. Sharpe J. Wolpert's French Flag: what's the problem? Development. 2019 Dec 20;146:dev185967. doi: 10.1242/dev.185967.

26. Crick F. Diffusion in embryogenesis. Nature. 1970 Jan 31;225(5231):420-2. doi: 10.1038/225420a0.

27. Bard JB. A model for generating aspects of zebra and other mammalian coat patterns. J Theor Biol. 1981 Nov 21;93(2):363-85. doi: 10.1016/0022-5193(81)90109-0.

503 28. Papageorgiou S, Almirantis Y. Gradient model describes the spatial-temporal expression pattern
504 of HOXA genes in the developing vertebrate limb. Dev Dyn. 1996 Dec ;207:461-469. doi:
505 10.1002/(SICI)1097-0177(199612)207:4<461::AID-AJA10>3.0.CO;2-4

506 29. Ben-Zvi D, Shilo BZ, Fainsod A, Barkai N. Scaling of the BMP activation gradient in Xenopus
507 embryos. Nature. 2008 Jun 26;453(7199):1205-11. doi: 10.1038/nature07059.

508 30. Raspopovic J, Marcon L, Russo L, Sharpe J. Modeling digits. Digit patterning is controlled by a
509 Bmp-Sox9-Wnt Turing network modulated by morphogen gradients. Science. 2014 Aug
510 1;345(6196):566-70. doi: 10.1126/science.1252960.

511 31. Grimm O, Coppey M, Wieschaus E. Modelling the Bicoid gradient. Development. 2010
512 Jul;137(14):2253-64. doi: 10.1242/dev.032409.

513 32. Yu SR, Burkhardt M, Nowak M, Ries J, Petrásek Z, Scholpp S, et al. Fgf8 morphogen gradient
514 forms by a source-sink mechanism with freely diffusing molecules. Nature. 2009 Sep
515 24;461(7263):533-6. doi: 10.1038/nature08391.

516 33. Lander AD, Nie Q, Wan FY. Do morphogen gradients arise by diffusion? Dev Cell. 2002
517 Jun;2(6):785-96. DOI: 10.1016/s1534-5807(02)00179-x.

518 34. Chara O, Tanaka EM, Brusch L. Mathematical modeling of regenerative processes. Curr Top Dev
519 Biol. 2014; 108:283-317. doi: 10.1016/B978-0-12-391498-9.00011-5.

520 35. Simpson MJ. Exact solutions of linear reaction-diffusion processes on a uniformly growing
521 domain: criteria for successful colonization. PLoS One. 2015 Feb 18;10(2):e0117949. doi:
522 10.1371/journal.pone.0117949.

523 36. Landman KA, Pettet GJ, Newgreen DF. Mathematical models of cell colonization of uniformly
524 growing domains. Bull Math Biol. 2003 Mar;65(2):235-62. doi: 10.1016/S0092-8240(02)00098-8.

525 37. Glazier JA, Graner F. Simulation of the differential adhesion driven rearrangement of biological
526 cells. Phys Rev E. 1993; 47: 2128–2154.

527 38. Savill NJ, Hogeweg P. Modelling Morphogenesis: From Single Cells to Crawling Slugs. J Theor Biol.
528 1996. doi: 10.1006/jtbi.1996.0237.

529 39. Swat MH, Thomas GL, Belmonte JM, Shirinifard A, Hmeljak D, Glazier JA. Multi-scale modeling
530 of tissues using CompuCell3D. Methods Cell Biol. 2012; 110:325-66. doi: 10.1016/B978-0-12-
531 388403-9.00013-8.

532 40. Starruß J, de Back W, Brusch L, Deutsch A. Morpheus: a user-friendly modeling environment for
533 multiscale and multicellular systems biology. Bioinformatics. 2014 May 1;30(9):1331-2. doi:
534 10.1093/bioinformatics/btt772.

535 41. Nagai T and Honda H. A dynamic cell model for the formation of epithelial tissues. Philos Mag B.
536 2001 Mar 24. doi: 10.1080/13642810108205772.

537 42. Farhadifar R, Röper JC, Aigouy B, Eaton S, Jülicher F. The Influence of Cell Mechanics, Cell-Cell
538 Interactions, and Proliferation on Epithelial Packing. 2007 Dec 18. Curr Biol. doi:
539 10.1016/j.cub.2007.11.049.

540 43. Mirams GR, Arthurs CJ, Bernabeu MO, Bordas R, Cooper J, Corrias A, et al. Chaste: An Open
541 Source C++ Library for Computational Physiology and Biology. PLoS Comput Biol. 2013 Mar 24;9(3):
542 e1002970. doi: 10.1371/journal.pcbi.1002970.

44. Harris CR, Millman KJ, van der Walt SJ, et al. Array programming with NumPy. Nature. 2020 Sep 16; 585,357–362. doi: 0.1038/s41586-020-2649-2.

45. Virtanen P, Gommers R, Oliphant TE, Haberland M, Reddy T, Cournapeau D, Burovski E, et al. SciPy 1.0: fundamental algorithms for scientific computing in Python. Nat Methods. 2020 Feb 3;17(3):261-272. doi: 10.1038/s41592-019-0686-2.

46. Hunter JD. Matplotlib: A 2D graphics environment. Comput Sci Eng. 2007 Jun 18;9:90–95.

47. Waskom, M. *et al*., 2017. mwaskom/seaborn: v0.8.1 (September 2017), Zenodo. Available at: doi:10.5281/zenodo.883859.

48. Ceccarelli A, Borges A, Chara O. Supplementary notebooks for Size matters: An analytical study of the role of tissue size in spatiotemporal distribution of morphogens unveils a transition between different Reaction-Diffusion regimes (Version v1.1); 2021 Jan 11. Zenodo. http://doi.org/10.5281/zenodo.4421327.